2013

Probing the bifunctional catalytic activity of ceria nanorods towards the cyanosilylation reaction

Gonghua Wang
University of Nebraska-Lincoln

Lu Wang
University of Nebraska at Omaha

Xiang Fei
University of Nebraska-Lincoln, xfei@huskers.unl.edu

Yunyun Zhou
University of Nebraska-Lincoln

Renat F. Sabirianov
University of Nebraska at Omaha, rsabirianov@mail.unomaha.edu

See next page for additional authors

Catalysis
Science & Technology

RSC Publishing

PAPER

View Article Online
View Journal | View Issue

Probing the bifunctional catalytic activity of ceria nanorods towards the cyanosilylation reaction†

Cite this: *Catal. Sci. Technol.*, 2013, **3**, 2602

Gonghua Wang,‡[a] Lu Wang,[b] Xiang Fei,*[a] Yunyun Zhou,[a] Renat F. Sabirianov,[b] Wai Ning Mei[a] and Chin Li Cheung*[a]

Received 23rd March 2013,
Accepted 24th May 2013

DOI: 10.1039/c3cy00196b

www.rsc.org/catalysis

Ceria nanorods were demonstrated to be an active, bifunctional catalyst for the cyanosilylation of aldehydes. The catalytic activity of ceria was shown to be positively correlated with a decrease in the coordination numbers of neighbouring oxygen atoms around cerium atoms in the catalyst. Chemisorption and density functional theory studies suggested that the coordinatively unsaturated cerium sites exposed by the surface oxygen vacancy defects functioned as Lewis acid sites and the neighbouring oxygen atoms behaved as Lewis base sites in the catalytic cycle.

1. Introduction

As an excellent oxygen source and storage medium, cerium oxide (ceria, or CeO_{2-x}, $0 < x \leq 0.5$) is widely used as a redox catalyst. Its chemical properties are closely related to the density of oxygen vacancy defect (OVD) sites in its crystal structure. Notably, ceria's capability of forming and eliminating intrinsic defects which depends on the high mobility of oxygen within its lattice structure has led to its variety of important catalytic applications.[1] Nano structured ceria typically exhibits high catalytic activity towards oxidative reactions due to its high density of surface OVDs, in contrast, bulk ceria which has nearly stoichiometric composition and possesses few structure defects is less catalytically active.[1a,2] By exploiting the nanosize effect, the OVD density of ceria nanostructures can be further enhanced using a previously demonstrated low vacuum annealing method[4] to create abundant superficial coordinatively unsaturated cerium sites.

While the relationship between the redox properties and OVD sites of ceria has been intensively studied, the nature of the dual acid–base characteristic of ceria and its connections to OVDs are seldom discussed in the literature. Ceria has been reported to chemisorb proton donors such as pyrroles, and electron acceptors such as carbon dioxide.[3] Such chemisorption characteristics of ceria indicate the possible presence of active Lewis acid and Lewis base sites on its surface.[3,4] Based on the local electronic structure around OVDs, namely the cerium atoms exposed by the surface OVDs and the nucleophilic, electron-rich oxygen atoms around the reduced cerium atoms, ceria can in principle possess bifunctional acid–base properties.[3]

Cyanosilylation of carbonyl compounds with trimethylsilyl cyanide is an important C–C bond formation reaction because the products, cyanohydrins, can be transformed into many value-added chemicals with functional groups including α-hydroxycarbonyl compounds and β-amino alcohols.[5] To date, heterogeneous catalysts reported for the cyanosilylation reactions typically contain Lewis acid sites and/or Lewis base sites such as mesoporous aluminosilicates,[6] cerium-containing metal–organic framework catalysts[7] and solid acids.[8] Thus, cyanosilylation can serve as a useful reaction to study the acid–base active centers of catalysts.

Herein, we report our study of the nature of bifunctional catalytic sites on ceria nanorods using the cyanosilylation of aldehydes as the probe reaction. Lewis acid and Lewis base sites on the surfaces of the ceria nanorods were produced by removing oxygen atoms in the samples using a low pressure thermal activation process developed by our group.[2b] Our study focuses on ceria nanorods because this activation process was found to be more effective on creating OVDs in ceria nanorods than ceria nanoparticles. To clarify the relationship between the catalytic activity of ceria and its active acid–base sites, we evaluate the catalytic activities of ceria nanorods and bulk ceria and correlate these findings with the average coordination numbers of neighboring oxygen atoms around cerium atoms

[a] *Department of Chemistry and Nebraska Centre for Materials and Nanoscience, University of Nebraska-Lincoln, Lincoln, NE 68588, USA. E-mail: ccheung2@unl.edu, xfei@huskers.unl.edu; Fax: +1-402-472-9402; Tel: +1-402-472-5172*

[b] *Department of Physics, University of Nebraska at Omaha, Omaha, NE 68182, USA*

† Electronic supplementary information (ESI) available: NMR spectra of the reaction products; TEM images and EXAFS data of ceria nanorods and bulk ceria; optimized structure, isosurfaces and charge analysis of the CeO_2, Ce_2O_3–CeO_2 and TMSCN–Ce_2O_3–CeO_2 slab by DFT calculations. See DOI: 10.1039/c3cy00196b

‡ Current address: Department of Mechanical and Materials Engineering, University of Nebraska-Lincoln, Lincoln, NE 68588, United States.

in these samples by extended X-ray absorption fine structure (EXAFS). Chemisorption studies and density functional density theory (DFT) modelling were further applied to investigate the structures and interactions between the reactants and the ceria surface, and elucidate a potential mechanistic pathway for the catalytic reactions.

2. Experimental procedures

2.1 Chemicals

All chemicals were purchased from Sigma-Aldrich (St. Louis, MO) and used without further purifications unless otherwise noted. A Millipore Synergy system was used to produce the deionized (DI) water of 18 MΩ cm resistivity.

2.2 Catalyst preparation

Ceria nanorods were synthesized using a reported hydrothermal method.[2b] Briefly, in a typical experiment, 0.5 g of cerium(III) sulphate hydrate was loaded into a 50 mL of Teflon-lined stainless steel autoclave (Parr Instrument, Moline, IL) and mixed with an aqueous sodium hydroxide solution (10 M, 40 mL) under stirring. The autoclave was then heated in a convection oven at 120 °C for 15 h. The resulting precipitated powder was collected by filtration with 3.0 μm track-etched membranes (Millipore, Billerica, MA) and rinsed with DI water. The resulting cerium(III) hydroxides nanorods were dried at 50 °C for 1 h for partial oxidation to yield a mixture of cerium(III) oxide and cerium(IV) oxide. Afterwards, the partially oxidized sample was crushed using a spatula and heated at 50 °C for another hour for further oxidation. The dried sample was then mixed with 100 mL of 15% v/v aqueous hydrogen peroxide (H_2O_2). The mixture was sonicated for 30 min, left still for 1 h, followed by filtration, rinsing with DI water and drying at 50 °C for 2 more hours. The obtained ceria nanorods were then activated *via* annealing for 30 min at 400 °C under vacuum at 0.1 Torr in a horizontal quartz tube furnace. Ceria nanorods without activation were also evaluated in the cyanosilylation study for comparisons.

Bulk cerium oxide powders (bulk ceria) (Alfa Aesar, Ward Hill, MA) were evaluated as-purchased. Note that these commercial samples were typically pre-treated or manufactured at high temperatures in air to ensure their stoichiometric ratio. Bulk ceria powders activated using conditions similar to those for the ceria nanorods were also used as controls for comparisons.

2.3 Catalyst evaluation using the cyanosilylation reaction

In a typical reaction, one of the aldehydes (0.5 mmol as listed in Table 1), deuterated chloroform ($CDCl_3$, 1.0 mL), trimethylsilyl cyanide (TMSCN, 0.6 mmol) and ceria catalyst (*ca.* 12.0 mg) were added into a capped glass vial at room temperature (22 °C) under constant magnetic stirring. Aliquots were taken periodically from these vials and filtered through a cotton plug to remove catalyst powders. ^{1}H-NMR spectra of the products in $CDCl_3$ were recorded on an NMR spectrometer (Avance 300 MHz, Bruker BioSpin Corporation, Billerica, MA). Chemical shifts are given in δ relative to tetramethylsilane. The yields of the reactions were calculated based on ^{1}H-NMR analysis of the products.

The regeneration of used catalysts was achieved by mixing 1 mL of aqueous H_2O_2 (30% v/v) with 50 mg of used catalysts for 5 min at room temperature. The treated sample was then filtered and washed with DI water, followed by low pressure thermal activation under the same activation conditions as in the catalyst preparation.

2.4 Catalyst impregnation treatments with trimethylsilyl cyanide and 4-methoxybenzaldehyde

Activated ceria catalysts were immersed in TMSCN and also 4-methoxybenzaldehyde (4-MBA) for 12 h. The residues were filtered off, rinsed with chloroform to remove the unbound TMSCN or 4-MBA and dried under vacuum. The resulting ceria nanorod catalysts impregnated with TMSCN or 4-MBA were denoted as ceria nanorods-TMSCN and ceria nanorods-4-MBA, respectively. The bulk ceria catalysts treated separately with each of TMSCN and 4-MBA were denoted as bulk ceria-TMSCN and bulk ceria-4-MBA, respectively.

2.5 Characterization methods

The morphology and crystal structures of the ceria nanorods and bulk ceria were examined by transmission electron microscopy (TEM) and X-ray diffractometry (XRD). The TEM images of ceria nanorods and bulk ceria were obtained using a Hitachi H7500 TEM (Hitachi High Technologies America, Inc., Dallas, TX) operated at 120 kV. Statistical dimension analysis of the particles/rods was based on more than 50 data points for each data set. The XRD patterns of the catalysts were obtained using a Bruker D8 Advance X-Ray Diffractometer (Bruker, Madison, WI) to examine their crystal structures. The weighted average wavelength of the Cu Kα X-ray source is 1.5417 Å. The surface areas of ceria nanorods and bulk ceria were determined using the Brunauer, Emmett, and Teller (BET) method using an ASAP 2010 Analyzer (Micromeritics, Norcross, GA).

The local atomic structures of the ceria samples were studied using the X-ray absorption fine structure (XAFS) technique. For the unactivated ceria nanorods, their Ce L_{III}-edge XAFS spectra were collected at the DCM beamline at the Center for Advanced

Table 1 Physical parameters of ceria nanorods and bulk ceria

	Ceria nanorods		Bulk ceria	
Physical parameters	Unactivated	Activated	As-purchased	Activated
Coordination number of Ce	7.0 ± 0.1	6.3 ± 0.1[a]	8.0 ± 0.1[a]	8.0 ± 0.1[a]
Surface area (m^2 g^{-1})	90	86	9.8	9.4

[a] Data from a previous study of an extended X-ray absorption fine structure for similarly produced ceria samples.[2b]

Microstructures and Devices (CAMD, Louisiana State University, Baton Rouge, LA). Monochromatic light was obtained using a double crystal monochromator of the Lemonnier type[2] equipped with a Ge(220) crystal pair for cerium. The estimated energy resolution was approximately 2 eV. Spectra were collected in the transmission mode using a Peltier-cooled Si (Li) detector for ceria samples under atmospheric pressure. At least two scans were collected to ensure reproducibility of the experimental data. The Ce L_{III}-edge XAFS data were analyzed by the FEFF-6 code.[9] The XAFS data of the activated ceria nanorods and bulk ceria were obtained from our previous investigation of samples using similar methods.[2b]

The Fourier transformed infrared (FT-IR) spectra of ceria nanorods and bulk ceria treated with either 4-MBA or TMSCN were acquired on a Nicolet Avatar 360 FT-IR equipped with the Smart Performer ATR accessory and a zinc selenide crystal (Thermo scientific, West Palm Beach, FL). The FTIR spectra of 4-MBA and TMSCN (98%) were also obtained for comparisons.

The oxidation states of Si, N, and Ce in each untreated and reactant-treated ceria nanorods and bulk ceria catalyst powders were examined by X-ray photoemission spectroscopy (XPS) (PHI 5000 Versa Probe scanning XPS Microprobe, Physical Electronics, Inc., Chanhassen, MN) at the University of North Texas. The instrument was calibrated using a gold standard. An aluminium anode X-ray source of 1486.6 eV was used. The survey spectra were acquired using a pass-energy of 187.85 eV with a resolution of 1 eV, while the high resolution spectra had a step-size of 0.2 eV and a pass-energy of 23.5 eV.

2.6 Computational modelling

DFT calculations for ceria (CeO_{2-x}) slab models without or with chemisorbed TMSCN were performed using the VASP code,[10] plane wave basis set with a cut-off energy of 400 eV, projector augmented-wave method[11] and generalized gradient approximation within the parameterization of Perdew–Burke–Ernzerhof.[12] The DFT + U method[13] was used for the corrections of on-site Coulomb interactions with U = 5 eV for Ce atoms. Mulliken population analysis[14] was applied to calculate the charge of an individual atom in the model. The ceria slab model was constructed with nine atomic layers of (111) CeO_2. 8% of oxygen atoms including several oxygen atoms in the surface and subsurface oxygen layers were removed from a stoichiometric CeO_2 model in order to simulate an oxygen-deficient ceria surface with both surface and subsurface oxygen vacancy defects. Geometry optimization was performed to determine the stable structure after one TMSCN molecule was chemisorbed on the surface. The calculated isosurfaces of electron density were false-color-coded with the electrostatic potential[15] and used to provide direct illustrations of the surface electron density of the ceria models and ones with adsorbed TMSCN. The negative electrostatic potential around oxygen-sites (or O-sites) illustrates that O atoms are negatively charged. Particularly, the surface O atoms are found to be even more negatively charged than the subsurface ones. The positive electrostatic potential around cerium-sites (or Ce-sites) suggests that the surface exposed Ce atoms are positively charged.

The calculated binding energy and charges of individual atoms are listed in Table S4 (ESI†). The binding energy of TMSCN chemisorbed on the defective ceria slab is defined as E(TMSCN–CeO_{2-x}) − E(TMSCN) − E(CeO_{2-x}), where E(TMSCN–CeO_{2-x}), E(TMSCN), and E(CeO_{2-x}) represent the total energies of TMSCN adsorbed on the CeO_{2-x} slab, TMSCN molecule, and CeO_{2-x} slab, respectively.

3. Results and discussion

3.1 Structure characterization of ceria nanorods and bulk ceria

The morphology and crystal structure of ceria nanorods and bulk ceria were analysed by XRD and TEM. TEM images of the ceria catalysts revealed that the ceria nanorods have diameters of 7 to 12 nm and lengths of 50 to 150 nm whereas the commercial bulk ceria particles have an average diameter of 101 ± 27 nm (Fig. 1 and Fig. S1, ESI†). There are no noticeable differences in the general morphology between the ceria samples before and after their activation treatment. The commercial bulk ceria exhibits much larger faceted structures with dimension of about ten times larger than that of ceria nanorods. From our experimental experience, these large faceted structures were only found in nanorod samples after calcination treatments at 900 °C or higher temperatures (data not shown). Thus, it is very likely that the as-purchased commercial bulk ceria have undergone high temperature calcination.

The XRD patterns of ceria nanorods and bulk ceria samples indicate that both ceria catalysts possess a cubic fluorite CeO_2 structure (Fig. S2, ESI†). Peak broadenings were observed in the XRD patterns of ceria nanorods when compared to the ones of bulk ceria. However, no obvious peak broadenings were noticed for the XRD patterns of the same ceria samples obtained before and after the activation process. This further corroborates with the TEM data that the activation process does not generate large morphological changes in the ceria samples.

Nonetheless, the low vacuum annealing activation process was found to increase the density of oxygen vacancy defects in ceria nanorods as revealed by the results of our present and previous EXAFS studies.[2b] The average coordination number of neighbouring O atoms around Ce atoms in unactivated ceria nanorods is 7.0 ± 0.1, whereas the corresponding value for

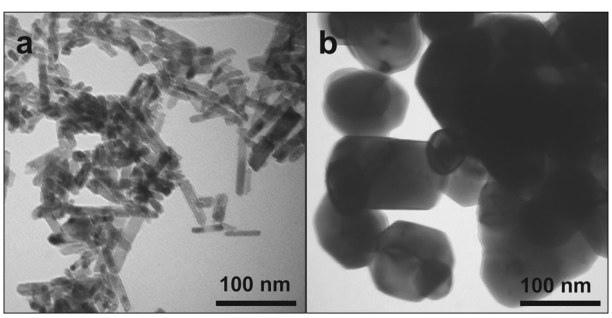

Fig. 1 TEM images of activated ceria catalysts. (a) Ceria nanorods and (b) bulk ceria.

activated ceria nanorods is 6.3 ± 0.1 (Table 1). These values are smaller than those for unactivated and activated bulk ceria (8.0 ± 0.1), or 8 for ideal fluorite-structured cerium(IV) oxide, suggesting the presence of higher density of oxygen vacancy defects. Clearly, the activated ceria nanorods exhibit higher OVD density than the unactivated ceria nanorods and this difference may cause large discrepancies in their catalytic activities (see Fig. S3 and Table S1, ESI† for detailed EXAFS fitting parameters). The indiscernible difference between the values of coordination numbers for bulk ceria before and after the activation indicates that the activation process has an insignificant impact on these samples.

The surface areas of ceria catalysts were measured to correlate this physical parameter with the catalytic activity of catalysts. The surface areas of activated and unactivated ceria nanorods were measured to be 90 $m^2 g^{-1}$ and 86 $m^2 g^{-1}$, respectively. The surface area of as-purchased and activated bulk ceria was determined to be 9.8 $m^2 g^{-1}$ and 9.4 $m^2 g^{-1}$. These measurements indicate that the annealing activation process has a minimal effect on decreasing the surface areas of both ceria catalysts.

3.2 Catalytic activity of ceria nanorods and bulk ceria

The catalytic activities of unactivated and activated ceria nanorods as well as that of bulk ceria were compared by monitoring the reaction conversion of the ceria-catalysed cyanosilylation of 4-methoxybenzaldehyde (4-MBA) using ^{1}H NMR (Fig. 2). We found that the activated ceria nanorod catalysed reaction preceded to completion in 3 h, while the one with unactivated ceria nanorods yielded only *ca.* 35% of the expected products in the same period of time. Very weak catalytic activities (less than 5% reaction yield or conversion) were found for both unactivated and activated bulk ceria after a 3 h period. The higher catalytic activity of activated ceria nanorods is positively correlated with the activation and the increased OVD density (or decreased average coordination number) in the ceria catalysts. The unactivated ceria nanorods and the two bulk ceria samples have lower OVD density than that of activated nanoceria because those three samples have larger coordination number values which are much closer to those of ideal CeO_2 structures (8). These catalysts were found to have much lower or no reaction activity over the 3 h reaction period. The distinctively different catalytic results cannot be solely attributed to the difference in the surface areas of ceria nanorods and bulk ceria. If the number of catalytically active sites is proportional to the surface area, since ceria nanorods and bulk ceria have surface areas of 90 $m^2 g^{-1}$ and 9.8 $m^2 g^{-1}$, respectively, the bulk ceria should exhibit some catalytic activity or at least 10% of the reaction yield with respect to that of activated ceria nanorods rather than that less the 5% reaction yield during and after the 3 h reaction period. Also, if the catalytic surface area argument is correct, the unactivated ceria nanorods should have exhibited a similar catalytic activity to the activated ceria rather than the obtained 35% reaction yield value.

We also investigated the catalytic activity of the activated ceria nanorods towards cyanosilylation reactions using nine other aromatic and aliphatic aldehyde substrates with different electron donating and withdrawing functional groups. We found that six out of the nine considered aldehydes achieved cyanosilylation completion within 1.5 h. The cyanosilylation of the remaining three aldehydes had over 90% yield in the first 1.5 h and attained full reaction completion in 3 h (Table 2, Fig. S4–S13, ESI†). Within this chosen reaction period, the different functional groups on these aldehydes seem to have little effect on the corresponding cyanosilylation reaction yields. This indicates excellent activation of aldehydes by the

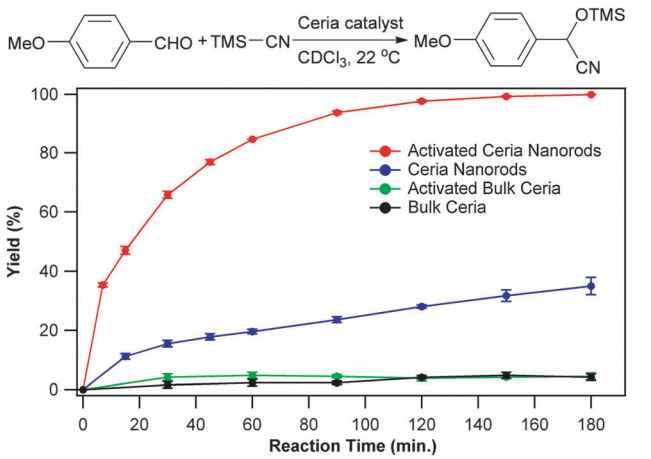

Fig. 2 Cyanosilylation of 4-MBA with TMSCN catalysed by ceria catalysts. Reaction conditions: The molar ratio of 4-MBA : TMSCN : ceria catalyst is 1 : 1.2 : 0.1. Reaction yields are based on NMR analysis.

Table 2 Results for the cyanosilylation of aldehydes using TMSCN catalysed by activated ceria nanorods at 22 °C

Entry	Aldehydes	Yield[a] (%) 1.5 h	3 h
1	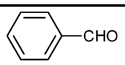	92	>99
2	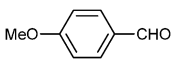	94	>99
3	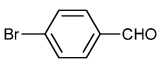	99	>99
4	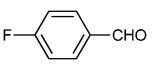	94	>99
5	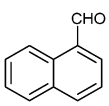	98	>99
6	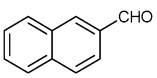	>99	—
7	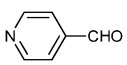	>99	—
8	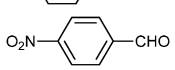	>99	—
9	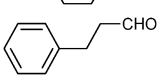	>99	—
10	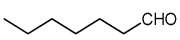	>99	—

[a] NMR yields. The molar ratio of R-CHO : TMSCN : activated ceria nanorods is 1 : 1.2 : 0.1.

activated ceria nanorods, compared to the other reported heterogeneous catalysis studies in which electron-withdrawing nitro group substituted aldehydes show relatively weaker activity.[16]

3.3 Probing catalyst–reactants interactions

Chemisorption studies were performed to investigate the Lewis basicity of the highly oxygen-deficient ceria nanorods by FT-IR and XPS. For comparisons, ceria nanorods and bulk ceria were separately impregnated with TMSCN and 4-MBA then rinsed with chloroform to remove unbound chemicals. To determine the chemical bonding environments of the ceria nanorod surface, 4-MBA and TMSCN, we performed FT-IR studied on TMSCN-treated and untreated ceria nanorods and pure TMSCN for comparisons (Fig. 3, Fig. S14 and S15, Table S2, ESI†). The characteristic peaks of the aldehyde group in 4-MBA, at 2740 cm^{-1} and 1680 cm^{-1}, correspond to the C–H stretch and C═O stretch respectively (Fig. 3a). While in the spectrum of the 4-MBA treated ceria nanorod catalyst, the C–H stretch peak diminished, and the C═O stretch peak is greatly suppressed. These changes indicate the chemisorption of 4-MBA onto the catalyst surface, likely *via* the carbonyl–metal interaction, with the ceria nanorod catalyst serving as Lewis acidic sites accepting electrons. None of the 4-MBA bonds were detected in the spectrum of 4-MBA treated bulk ceria.

The FT-IR spectra for TMSCN and TMSCN treated ceria catalyst revealed strong interactions between this reactant and the catalyst (Fig. 3b). The spectrum of free TMSCN typically displays a C≡N stretching peak at 2190 cm^{-1}.[8] In the spectrum of TMSCN-treated ceria nanorods, this C≡N stretching peak was red-shifted to 2166 cm^{-1}, suggesting the presence of weakened C≡N bonds. The chemisorption of TMSCN on ceria nanorods was supported by the shift of Si-related absorption peaks. In the spectrum of TMSCN, a Si–O–Si stretch at 1055 cm^{-1} is identified, attributed to the formed impurity of TMS–O–TMS because of the TMSCN self-degradation. In the spectrum of TMSCN-treated ceria nanorods, this peak is missing; instead, an extra peak emerges in the finger-print region at 912 cm^{-1}, which is usually attributed to the silanol Si–O stretch mode. Likely, either an oxygen atom or a hydroxyl group on the surface of the ceria nanorod catalyst may have undergone nucleophilic attack to the Si of TMSCN to form this Si–O bond. This bonding motif can possibly be realized by the coordination of the oxygen atom in the ceria nanorod surface to the silicon atom in TMSCN, or the formation of a possible hypervalent silicon intermediate *via* a Lewis base catalysed mechanism.[17] It is as similar as in the case of 4-MBA, little or no detected TMSCN bound onto the bulk ceria.

XPS data were employed to further examine the chemical structure of ceria nanorods and bulk ceria after the TMSCN-impregnation treatment. As shown in Fig. 4a, all spectra for the ceria samples have peak features indicating the presence of Ce and O. Typically, the presence of Si is revealed by the presence of the Si $2p_{1/2}$ and $2p_{3/2}$ peaks at a binding energy of around 99–100.5 eV. Also, though the FT-IR data suggested low concentration of Si on the TMS-ceria nanorod surface, no peaks were observed in this region of the XPS spectra (Fig. 4a and b).

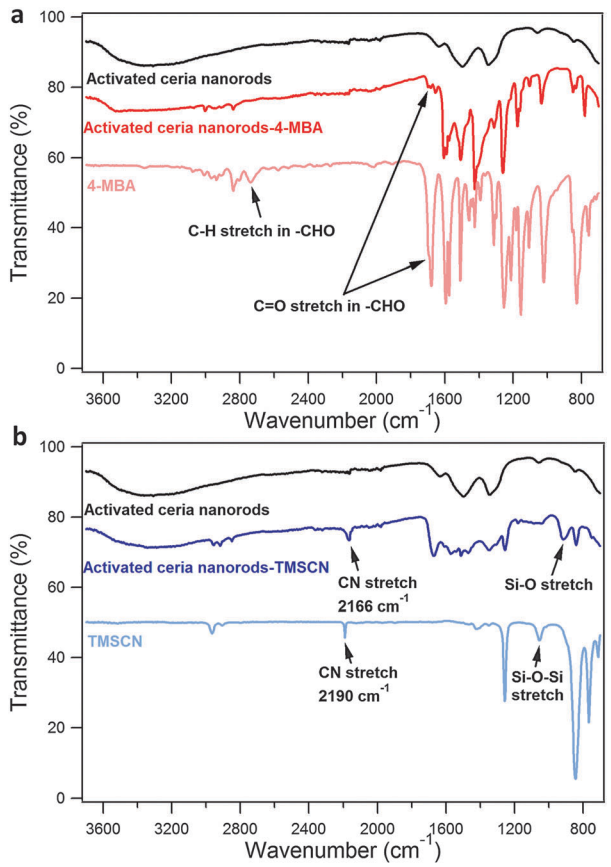

Fig. 3 FTIR spectra of activated ceria nanorods before and after impregnation in 4-MBA (a) and TMSCN (b). The spectra of 4-MBA and TMSCN are displayed for comparisons. The spectra are shifted downward for presentation clarity.

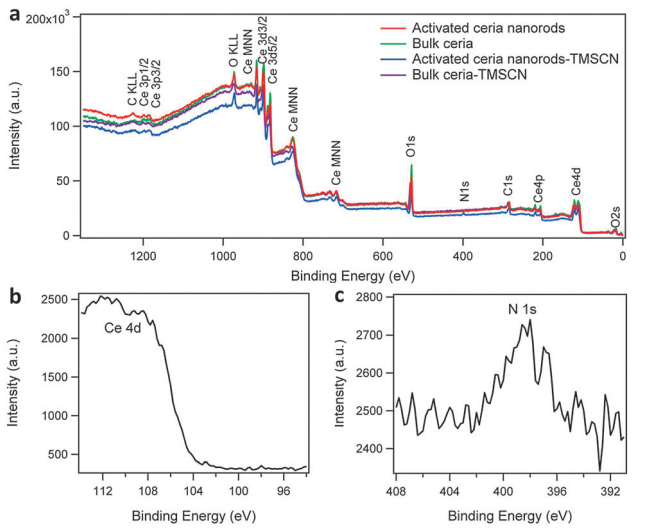

Fig. 4 (a) XPS spectra of the untreated and the TMSCN-treated ceria nanorods and bulk ceria catalysts, high resolution scans of (b) the expected Si 2p region of TMSCN-treated ceria nanorods and (c) N 1s spectrum of TMSCN-treated ceria nanorods.

There are two possible reasons. First, likely, the content of Si in the sample may be so low that it is below the detection limit of the XPS technique. Second, even if the Si 2p peaks are present in the corresponding XPS spectrum, they could be over-shadowed by the high intensity of the neighbouring Ce 4d peak ($4d_{3/2}$ at 112 eV and $4d_{5/2}$ at 109 eV).[18] In contrast, a weak peak at a binding energy of *ca.* 398 eV, which is commonly assigned to the binding energy of N 1s core,[18] was observed in the spectrum (Fig. 4c). This N 1s XPS signal corroborates the presence of CN functional groups in ceria nanorods-TMSCN as shown in FTIR data (Fig. 3b). Hence, the combined XPS and IR studies validate the chemisorption of TMSCN on the Lewis base sites on activated ceria nanorods.

3.4 Recyclability of ceria nanorod catalysts

The recyclability of ceria nanorod catalyst was evaluated using the cyanosilylation of 4-MBA reaction with TMSCN. As discussed in Section 3.2, the product yield of freshly made catalyst after a 3 h reaction is *ca.* 100%. Under the same reaction conditions, one sample catalyst presented a 62.5% product yield after the second round of reaction and a 25.4% product yield after the third round of reaction. The colour of the catalyst became darker purple after each use. As revealed by our chemisorption studies, this colour change was likely attributed to the binding of trimethylsilyl groups to the ceria surface. The partial deactivation of ceria nanorod catalysts after each use can be explained by the binding of excessive trimethylsilyl groups *via* a Si–O bond to the catalyst surface, consequent reduction of surface active sites and possible blocking of Ce^{3+} Lewis acid sites by these surface-bound trimethylsilyl groups on the catalyst surface.

The regeneration of used ceria nanorod catalysts was found to be achievable by treating the catalysts with aqueous H_2O_2 solution, followed by washing with DI water and low pressure (0.1 Torr) thermal activation at 400 °C. The regenerated catalyst possessed a pale yellow colour, similar to that of freshly prepared catalysts. They were found to exhibit $\geq$98% of their original catalytic activity towards the 3 h cyanosilylation of 4-MBA reaction. The addition of the hydrogen peroxide to the used catalysts typically yielded rapid evolution of gas bubbles. Likely, sufficient hydroxyl radicals or ions generated from the decomposition of hydrogen peroxide acted as nucleophiles to attack the silicon of the chemisorbed trimethylsilyl groups on the used ceria surface and consequently detached these surface "contaminants". Note that we did not find such regeneration treatment increase in the catalytic activity of bulk ceria. Detailed potential regeneration reaction mechanisms are still being studied.

3.5 Computational modelling

DFT calculations were performed to determine the influence of the oxygen vacancy defects on the Lewis basicity of ceria nanorods and the chemisorption of TMSCN on the catalyst surface. A 9-atomic-layered CeO_2 slab model with 8% of oxygen atoms removed from the surface and subsurface layers was constructed and optimized to simulate a CeO_{2-x} (111) surface containing both surface and subsurface OVDs (Fig. 5a and b, Fig. S16, ESI†). Electrostatic potential mappings of these structures reveal that the surface oxygen atoms around the OVD sites of the CeO_{2-x} slab are more electron-rich than surface oxygen atoms away from the OVD sites and the ones in the slab model without OVDs (Fig. 5c and d and Fig. S16, ESI†).

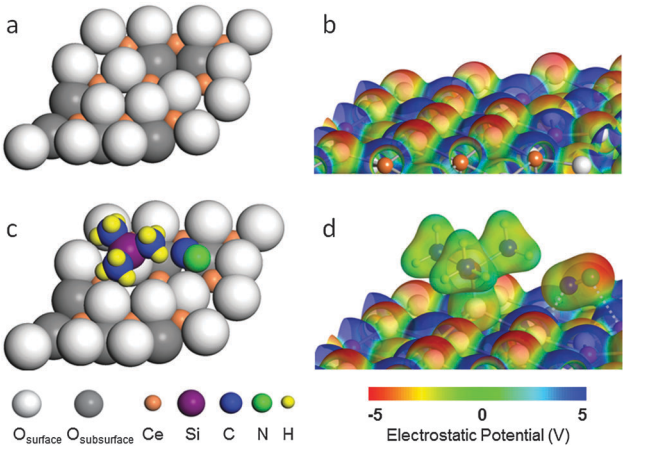

Fig. 5 Optimized structures of (a) CeO_{2-x} slab and (c) a TMSCN molecule adsorbed on the CeO_{2-x} slab. (b) and (d) are top views of electrostatic potential map of these two corresponding structures.

The optimized structure of a TMSCN molecule chemisorbed on the CeO_{2-x} slab surface illustrates that the absorbed TMSCN underwent bond-breaking and bond-formation (Fig. 5c and d, Fig. S16 and S17, ESI†). The calculated binding energy of a TMSCN molecule adsorbed on the ceria nanorod surface was −1.08 eV, suggesting the adsorption of TMSCN to be an exothermic reaction. In this optimized structure, the Si–C bond of the TMSCN was broken to form TMS and CN molecular fragments. The TMS moiety was bonded to the slab surface *via* a new Si–O bond formed by a surface O bound to subsurface Ce atoms around an OVD with a bond length of 1.68 Å (Fig. S17, ESI†). When compared to the CeO_{2-x} slab model, this TMS-bonded O atom and the three subsurface Ce atoms it bonded to were found to have the corresponding O–Ce bond lengths increased from 2.48, 2.37, and 2.49 Å to 2.61, 2.62, and 2.74 Å (Table S3, ESI†). The lengthened Ce–O bonds suggest a significant charge transfer from the TMS-bonded O atom to the TMS molecular fragment. The "detached" CN moiety from the chemisorption of TMSCN was likely trapped and weakly coordinated to the adjacent subsurface Ce atoms at the OVD. Mulliken population analysis revealed that 0.32 electrons were transferred from the ceria surface to the CN group (Table S4, ESI†).

Our calculation results suggest that upon the chemisorption of TMSCN onto the CeO_{2-x} slab in our experiments, the electron-rich surface O atoms around surface OVDs likely underwent a nucleophilic attack to the slightly positively charged Si from TMSCN and released CN^-, demonstrating the Lewis basicity of the oxygen-deficient ceria nanorod surface. Though our simulated model predicts a possible TMSCN binding motif to an oxygen deficient ceria surface, the implications of the DFT calculation results may be limited as the trapped oxygen

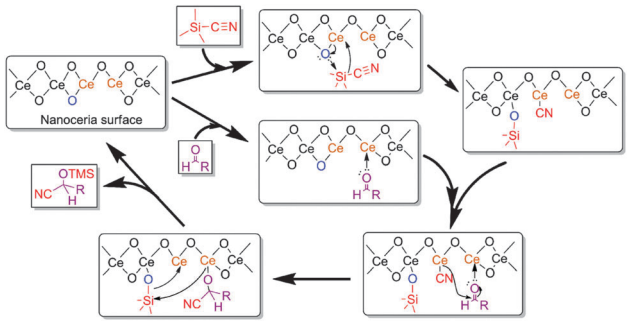

Fig. 6 A proposed mechanism for the cyanosilylation of an aldehyde catalysed by ceria nanorods with high oxygen vacancy defect density.

species, or the quasi-free electrons were not included in the models for the calculations.

3.6 Proposed catalytic mechanism

Based on the presented investigations, we postulate that the ceria nanorod catalysed cyanosilylation of aldehydes is likely attributed to the high density of Ce(III) sites (Lewis acid sites) and electron-rich neighbouring oxygen atoms (Lewis base sites) on the nanorod surface. A plausible mechanism of ceria nanorod-assisted cyanosilylation is depicted in Fig. 6. The electron-rich nucleophilic oxygen atoms on the ceria nanorod surface acted as Lewis bases and donated electrons to the trimethylsilyl group of TMSCN, forming coordinated Si–O bonds. This hypothesized that the pentavalent silicon intermediate likely has a weakened C–Si bond, resulting in the increase in nucleophilicity of the cyanide group, which is then released and bound to the adjacent Ce(III) sites. An aldehyde is activated to be more electrophilic through coordinating the Lewis acidic Ce(III) sites and forming a chemisorbed surface alkoxide. The nucleophilic attack of neighbouring cyanide to the polarized carbonyl group then proceeds due to the decreased activation barrier caused by the activated electrophile and nucleophile. The turnover of the catalyst is realized by the nucleophilic attack of the oxygen of the cerium-bound alkoxide intermediate to the TMS group followed by the release of the cyanosilylated product.

4. Conclusions

In summary, ceria nanorods with high oxygen vacancy defect density were demonstrated to exhibit high Lewis acid–base catalytic activity towards the cyanosilylation of aldehydes when compared to its bulk counterpart. Spectroscopic and computational modelling studies imply that the activation of TMSCN was likely initiated by the electron transfer from the electron-rich O atoms on the ceria nanorod surface (Lewis base sites) to the trimethylsilyl group of TMSCN. The coordinatively unsaturated Ce(III) sites present on the surface of oxygen-deficient ceria nanorods (weak Lewis acid sites) likely accounted for the activation of the carbonyl groups of the aldehydes by forming the surface-bound alkoxide moieties. The proposed mechanism was corroborated by the binding energy calculation results of the reactants on the oxygen-deficient ceria surface. This bifunctional ceria oxide catalyst does not only provide an interesting catalyst platform of heterogeneous catalysis for a variety of organic reactions, but also exemplifies an effective engineering strategy for designing active metal oxide catalysts.

Acknowledgements

We thank Nebraska Research Initiative, Army Research Office (W911NF-10-2-0099), NSF-EPSCoR (EPS-1010674) and DOE (DE-EE0003172) for their financial support. The University of Nebraska Holland Computing Center has provided computational resources with the associated USCMS Tier-2 site at the University of Nebraska-Lincoln. The spectroscopic materials characterization was partially supported by the Pennsylvania State University Materials Research Institute Nanofabrication Lab and the National Science Foundation Cooperative Agreement (ECS-0335765). We also thank the Center of Advanced Micro Devices at the Louisianan State University and the University of North Texas for the use of their facilities.

Notes and references

1 (*a*) F. Esch, S. Fabris, L. Zhou, T. Montini, C. Africh, P. Fornasiero, G. Comelli and R. Rosei, *Science*, 2005, **309**, 752–755; (*b*) P. Patsalas, S. Logothetidis, L. Sygellou and S. Kennou, *Phys. Rev. B: Condens. Matter Mater. Phys.*, 2003, **68**, 035104; (*c*) X. L. Song, G. Z. Qiu and P. Qu, *Rare Met. Mater. Eng.*, 2004, **33**, 29–34; (*d*) A. Trovarelli, *Catal. Rev.*, 1996, **38**, 439–520.

2 (*a*) K. B. Zhou, X. W. Liu, L. Wang, B. Y. Wang and Y. D. Li, *J. Am. Chem. Soc.*, 2009, **131**, 3140–3141; (*b*) N. J. Lawrence, J. R. Brewer, L. Wang, T. S. Wu, J. M. Wells-Kingsbury, M. M. Ihrig, G. Wang, Y. L. Soo, W. N. Mei and C. L. Cheung, *Nano Lett.*, 2011, **11**, 2666–2671.

3 L. Vivier and D. Duprez, *ChemSusChem*, 2010, **3**, 654–678.

4 C. Binet, M. Daturi and J. C. Lavalley, *Catal. Today*, 1999, **50**, 207–225.

5 J. M. Brunel and I. P. Holmes, *Angew. Chem., Int. Ed.*, 2004, **43**, 2752–2778.

6 K. Iwanami, J. C. Choi, B. W. Lu, T. Sakakura and H. Yasuda, *Chem. Commun.*, 2008, 1002–1004.

7 D. B. Dang, P. Y. Wu, C. He, Z. Xie and C. Y. Duan, *J. Am. Chem. Soc.*, 2010, **132**, 14321–14323.

8 B. Thirupathi, M. K. Patil and B. M. Reddy, *Appl. Catal., A*, 2010, **384**, 147–153.

9 J. J. Rehr, J. Mustre de Leon, S. I. Zabinsky and R. C. Albers, *J. Am. Chem. Soc.*, 1991, **113**, 5135–5140.

10 G. Kresse and J. Hafner, *Phys. Rev. B: Condens. Matter Mater. Phys.*, 1994, **49**, 14251–14269.

11 P. E. Blochl, *Phys. Rev. B: Condens. Matter Mater. Phys.*, 1994, **50**, 17953–17979.

12 J. P. Perdew, K. Burke and M. Ernzerhof, *Phys. Rev. Lett.*, 1996, **77**, 3865–3868.

13 S. L. Dudarev, G. A. Botton, S. Y. Savrasov, C. J. Humphreys and A. P. Sutton, *Phys. Rev. B: Condens. Matter Mater. Phys.*, 1998, **57**, 1505–1509.
14 R. S. Mulliken, *J. Chem. Phys.*, 1955, **23**, 1833–1840.
15 K. Momma and F. Izumi, *J. Appl. Crystallogr.*, 2011, **44**, 1272–1276.
16 W. K. Cho, J. K. Lee, S. M. Kang, Y. S. Chi, H. S. Lee and I. S. Choi, *Chem.–Eur. J.*, 2007, **13**, 6351–6358.
17 (*a*) S. E. Denmark and W. J. Chung, *J. Org. Chem.*, 2006, **71**, 4002–4005; (*b*) J. Gawronski, N. Wascinska and J. Gajewy, *Chem. Rev.*, 2008, **108**, 5227–5252.
18 J. F. Moulder, W. F. Stickle, P. E. Sobol and K. D. Bomben, *Handbook of X-ray Photoelectron Spectroscopy*, Perkin-Elmer Corporation Physical Electronics Division, Eden Prairie, Minnesota, 1992.

Electronic Supplementary Material (ESI) for Catalysis Science & Technology

Electronic Supplementary Information

Probing the bifunctional catalytic activity of ceria nanorods towards the cyanosilylation reaction

Gonghua Wang,[a, †] Lu Wang,[b] Xiang Fei,[a, *] Yunyun Zhou,[a] Renat F. Sabirianov,[b] Wai Ning Mei[b] and Chin Li Cheung[a, *]

[a]*Department of Chemistry and Nebraska Centre for Materials and Nanoscience, University of Nebraska-Lincoln, Lincoln, NE 68588, United States.*

[b]*Department of Physics, University of Nebraska at Omaha, Omaha, NE 68182, United States*

[†] *Current address: Department of Mechanical and Materials Engineering, University of Nebraska-Lincoln, Lincoln, NE 68588, United States.*

[*]*Phone: 1-402-472-5172; Fax: 1-402-472-9402; Email: ccheung2@unl.edu; xfei@huskers.unl.edu*

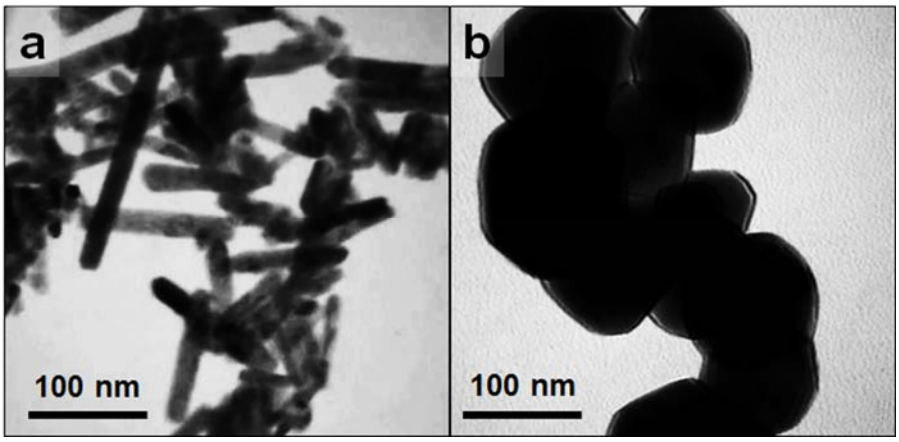

Fig. S1 TEM images of ceria catalysts before activation: (a) as-synthesized ceria nanorods and (b) as-purchased bulk ceria.

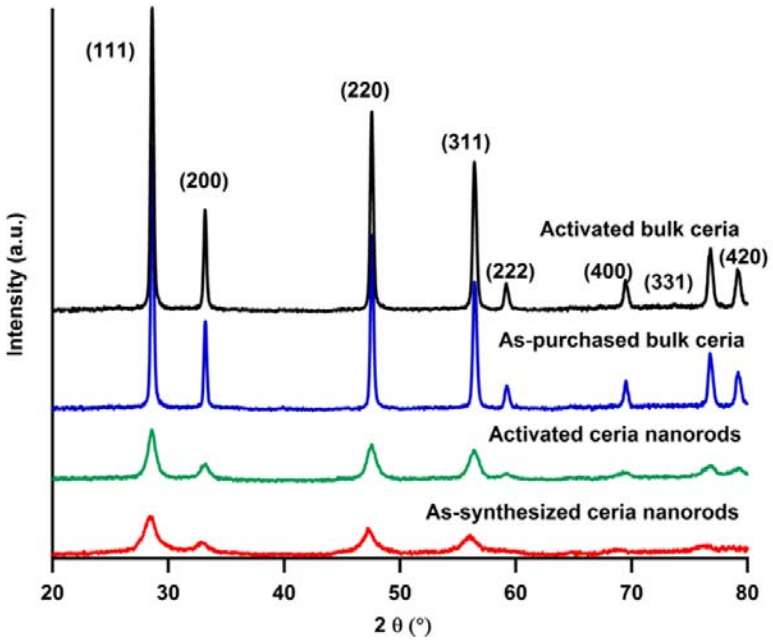

Fig. S2 XRD patterns of ceria catalysts: (red) as-synthesized ceria nanorods, (green) activated ceria nanorods, (blue) as-purchased bulk ceria and (black) activated bulk ceria. XRD peaks are indexed according to ICDD card 04-013-4361 with respect to the cubic $Fm\bar{3}m$ structure of cerium (IV) oxide (CeO_2).

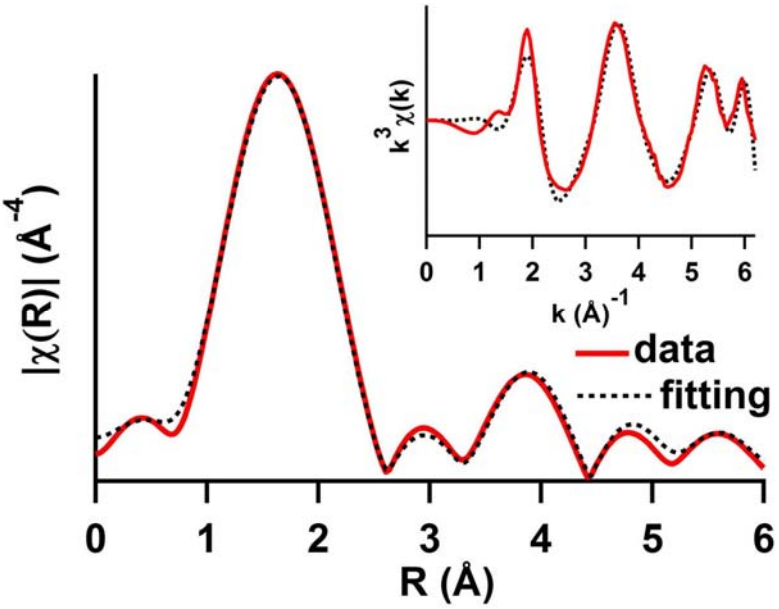

Fig. S3 Fourier transformed Ce L_3-edge EXAFS data of unactivated ceria nanorods. The inset data are the corresponding EXAFS functions in *k* space. (Red lines: data; black dotted lines: fittings.)

Table S1 Parameters of the local structure around Ce atoms obtained from curve fitting of the Ce L_{III}-edge EXAFS for unactivated and activated ceria nanorods and bulk ceria.

Sample	**Bond**	**N**	**R (Å)**	**σ (10^{-3} Å^2)**	**ΔE (eV)**
Unactivated ceria nanorods	Ce-O	7.0 ± 0.1	2.11 ± 0.01	8.7± 1.5	-0.84 ± 0.57
	Ce-Ce	7.7 ± 0.2	3.92 ± 0.02	17.4 ± 5.2	-2.68± 1.51
	Ce-O	18.4 ± 2.1	4.44 ± 0.02	15.1 ± 4.9	-1.68 ± 0.14
Activated ceria nanorods[a]	Ce-O	6.3 ± 0.1	2.29 ± 0.01	2.4 ± 0.2	2.5 ±0.2
	Ce-Ce	7.4 ± 0.4	3.82 ± 0.01	2.2 ± 0.5	-0.2 ± 0.4
	Ce-O	14.7 ± 1.2	4.52 ± 0.01	3.4 ± 0.5	0.8 ± 0.4
Bulk ceria[a]	Ce-O	8.0 ± 0.1	2.32 ± 0.01	0.1 ± 0.2	5.8 ± 0.2
	Ce-Ce	12.0 ± 0.3	3.82 ± 0.01	0.1 ± 0.5	-0.8 ± 0.4
	Ce-O	24.0 ± 1.2	4.48 ± 0.01	1.5 ± 0.5	1.6 ± 0.4

Notes: [a] Data for similarly prepared samples reported in reference 2b of the text.

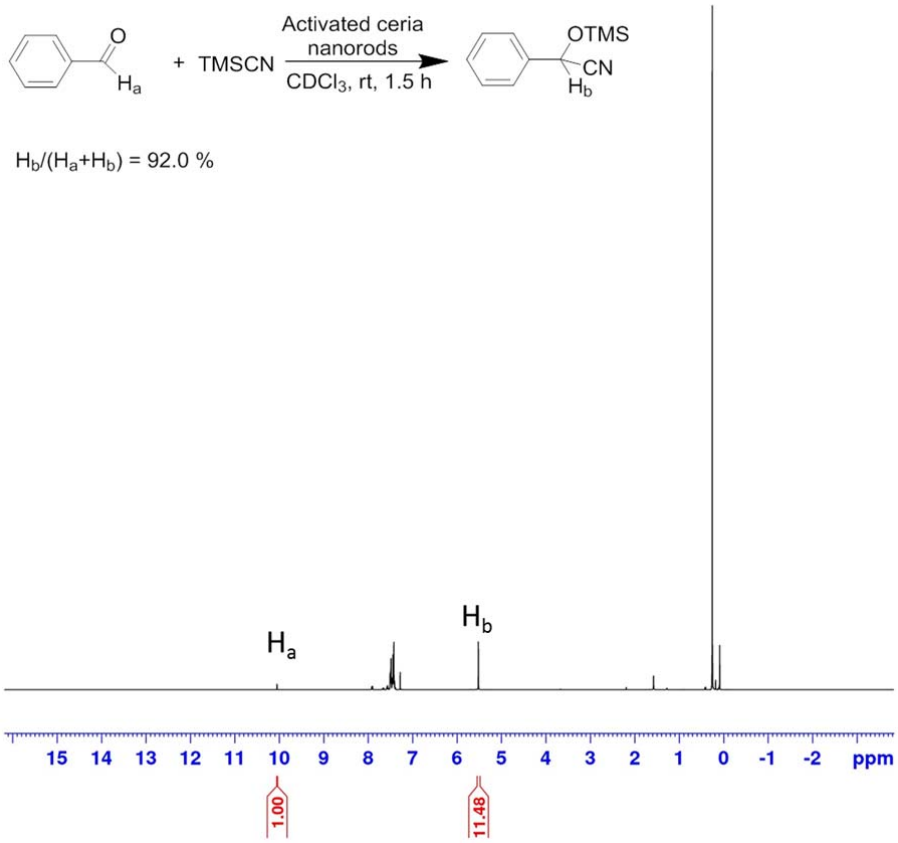

Fig. S4 NMR spectrum of the reaction mixture for reaction between benzaldehyde and TMSCN in Table 2 Entry 1 catalyzed by activated ceria nanorods after 1.5 hours of reaction time.

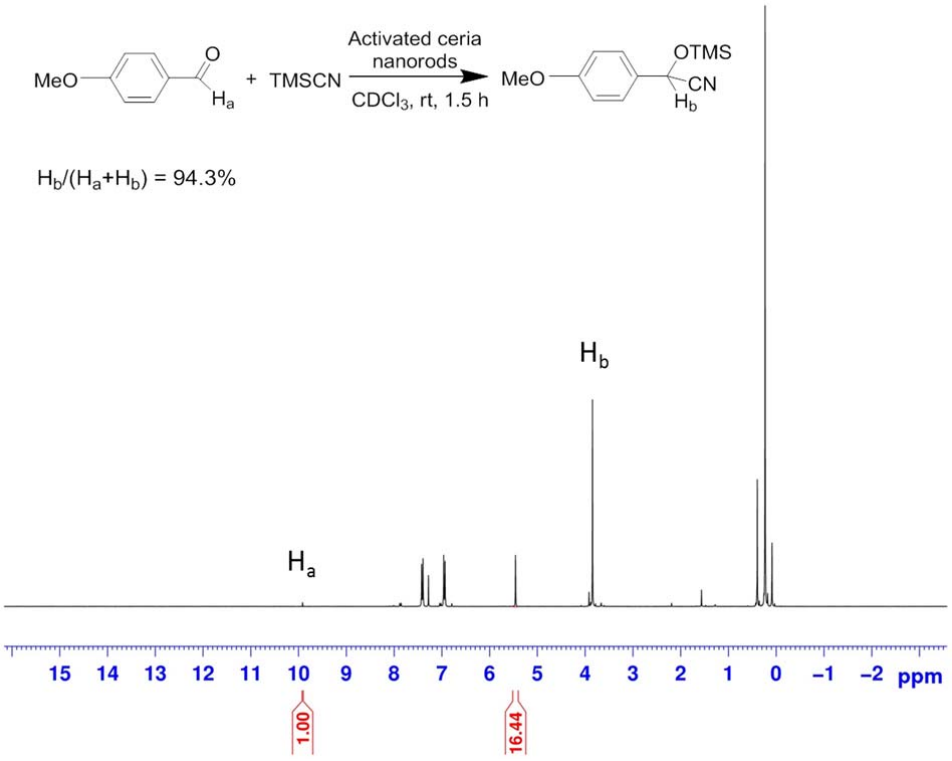

Fig. S5 NMR spectrum of the reaction mixture for reaction between 4-methoxybenzaldehyde and TMSCN in Table 2 Entry 2 catalyzed by activated ceria nanorods after 1.5 hours of reaction time.

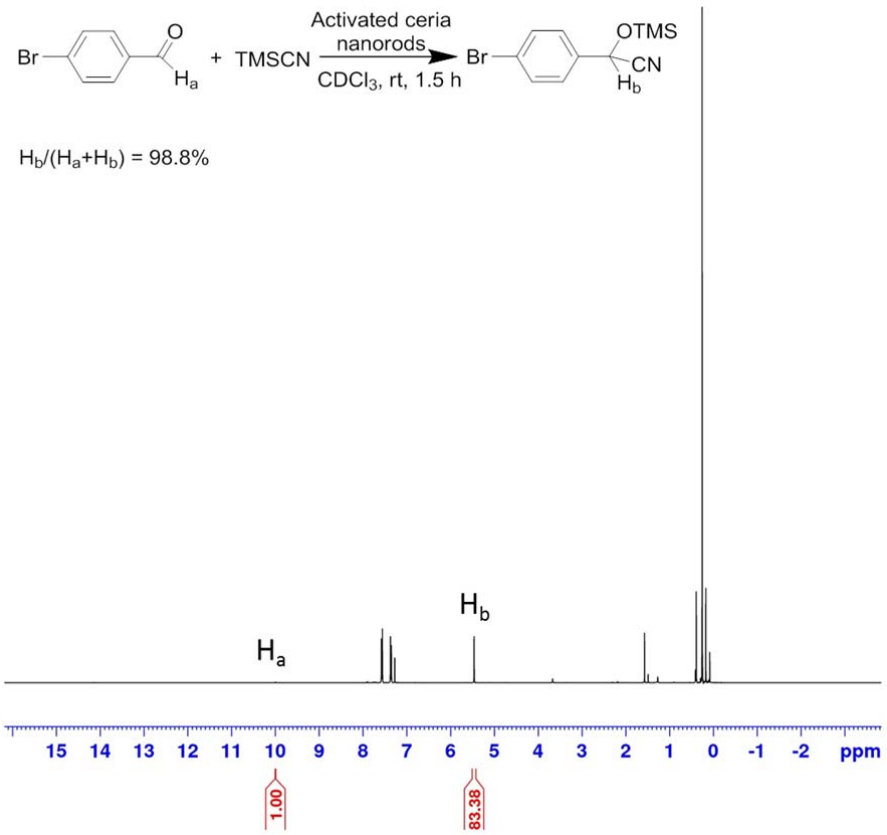

Fig. S6 NMR spectrum of the reaction mixture for reaction between 4-bromobenzaldehyde and TMSCN in Table 2 Entry 3 catalyzed by activated ceria nanorods after 1.5 hours of reaction time.

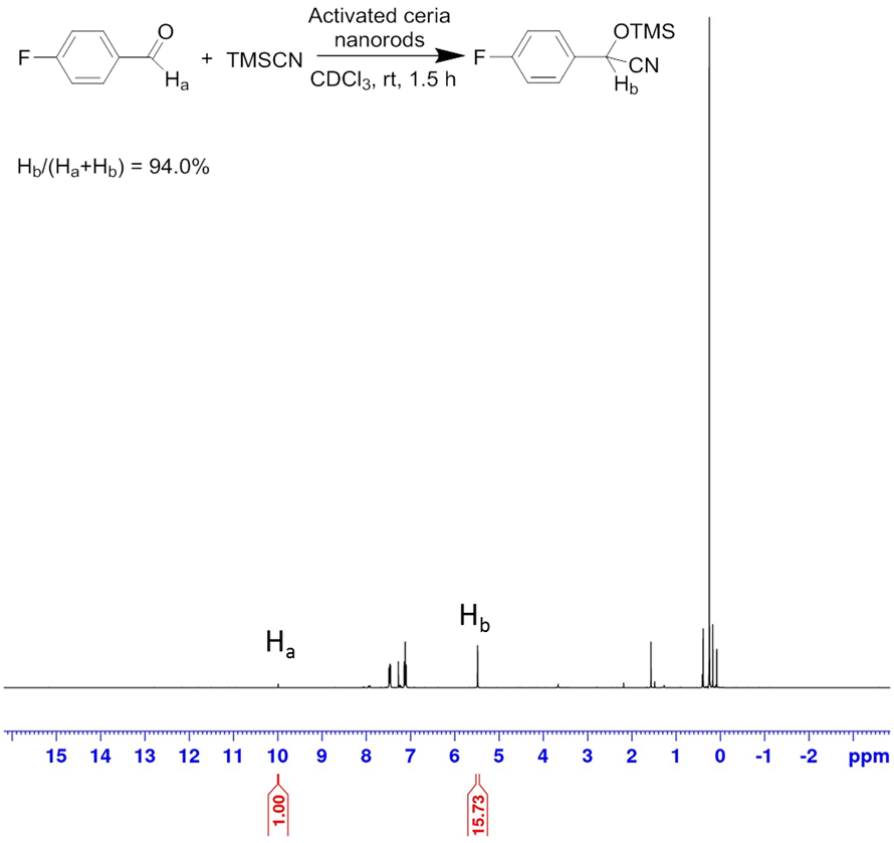

Fig. S7 NMR spectrum of the reaction mixture for reaction between 4-fluorobenzaldehyde and TMSCN in Table 2 Entry 4 catalyzed by activated ceria nanorods after 1.5 hours of reaction time.

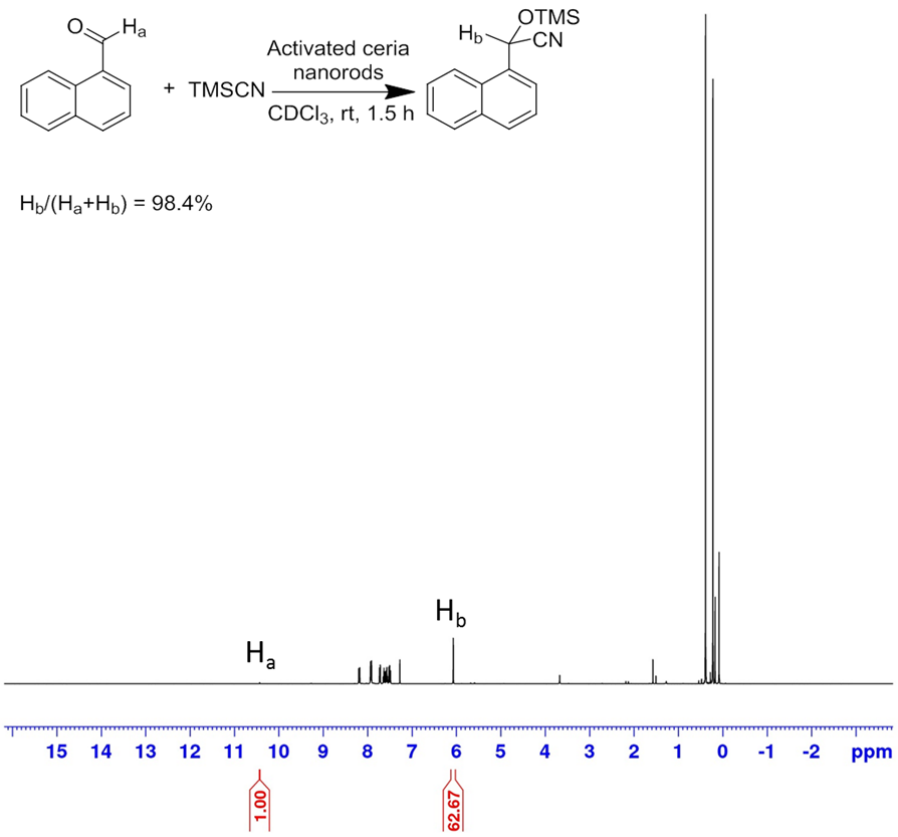

Fig. S8 NMR spectrum of the reaction mixture for reaction between 1-naphthaldehyde and TMSCN in Table 2 Entry 5 catalyzed by activated ceria nanorods after 1.5 hours of reaction time.

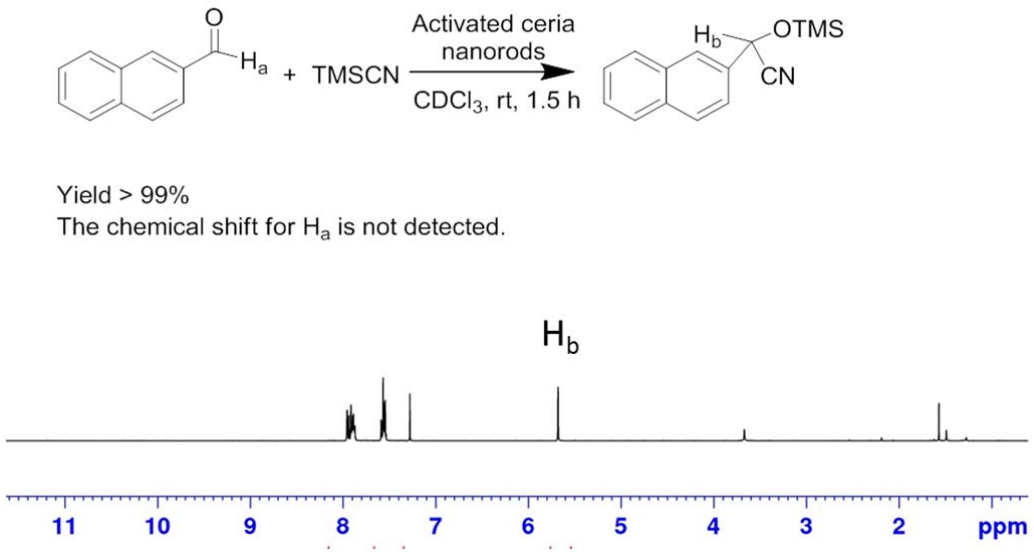

Fig. S9 NMR spectrum of the reaction mixture for reaction between 2-naphthaldehyde and TMSCN in Table 2 Entry 6 catalyzed by activated ceria nanorods after 1.5 hours of reaction time.

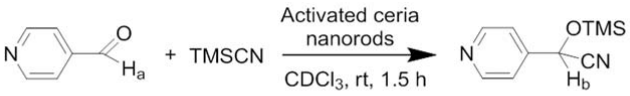

Yield > 99%
The chemical shift for H_a is not detected.

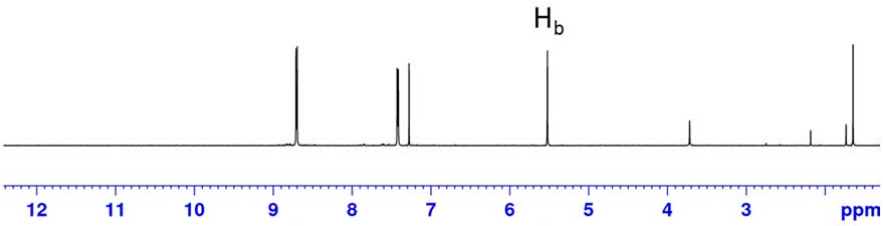

Fig. S10 NMR spectrum of the reaction mixture for reaction between isonicotinaldehyde and TMSCN in Table 2 Entry 7 catalyzed by activated ceria nanorods after 1.5 hours of reaction time.

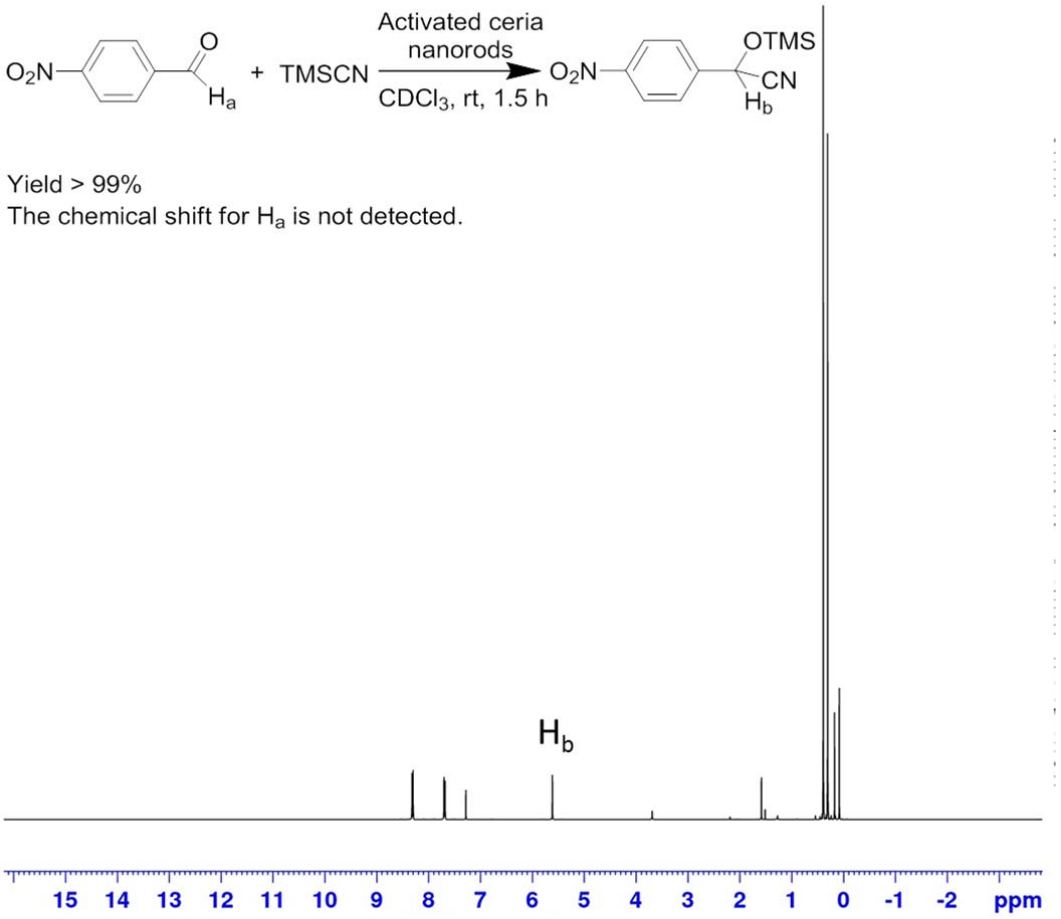

Fig. S11 NMR spectrum of the reaction mixture for reaction between 4-nitrobenzaldehyde and TMSCN in Table 2 Entry 8 catalyzed by activated ceria nanorods after 1.5 hours of reaction time.

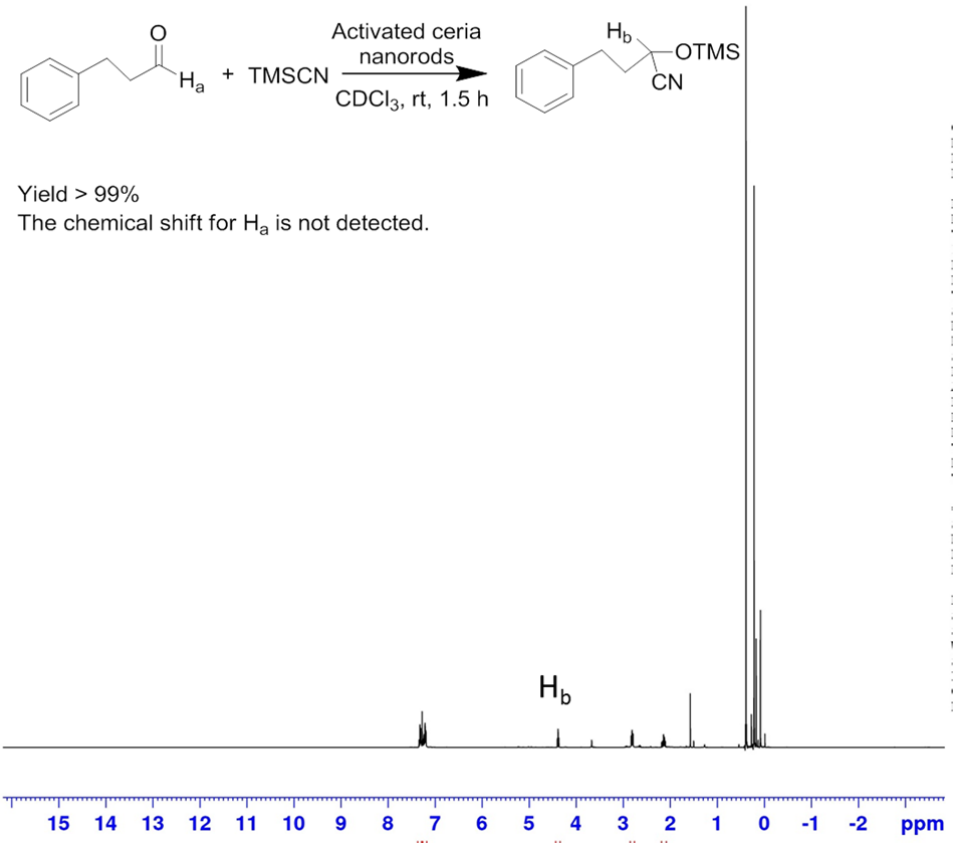

Fig. S12 NMR spectrum of the reaction mixture for reaction between 3-phenylpropanal and TMSCN in Table 2 Entry 9 catalyzed by activated ceria nanorods after 1.5 hours of reaction time.

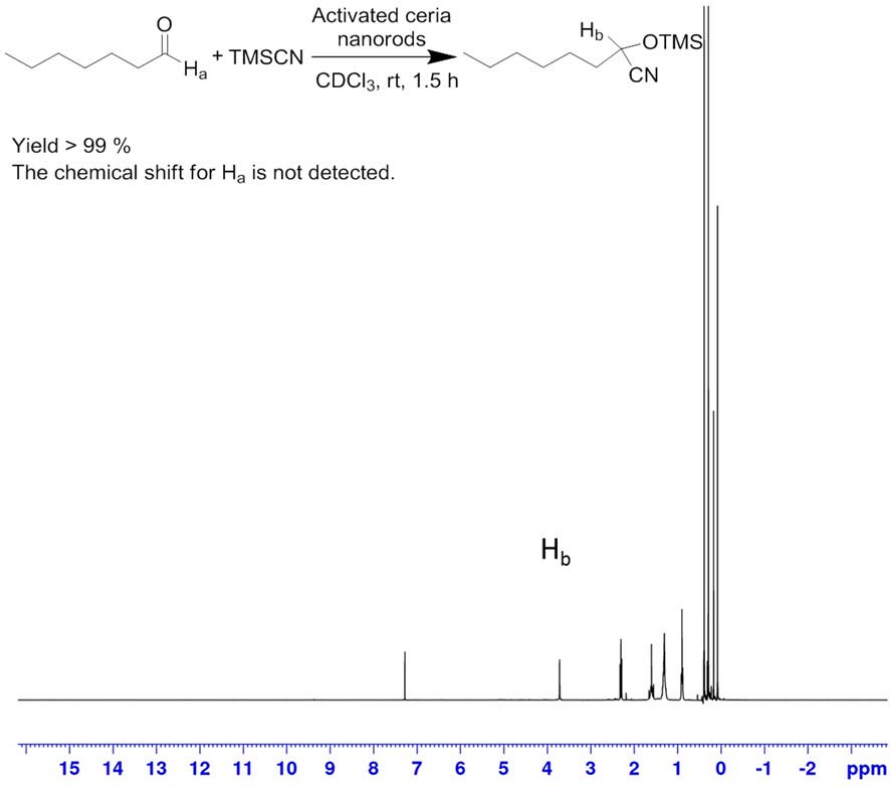

Fig. S13 NMR spectrum of the reaction mixture for reaction between heptanal and TMSCN in Table 2 Entry 10 catalyzed by activated ceria nanorods after 1.5 hours of reaction time.

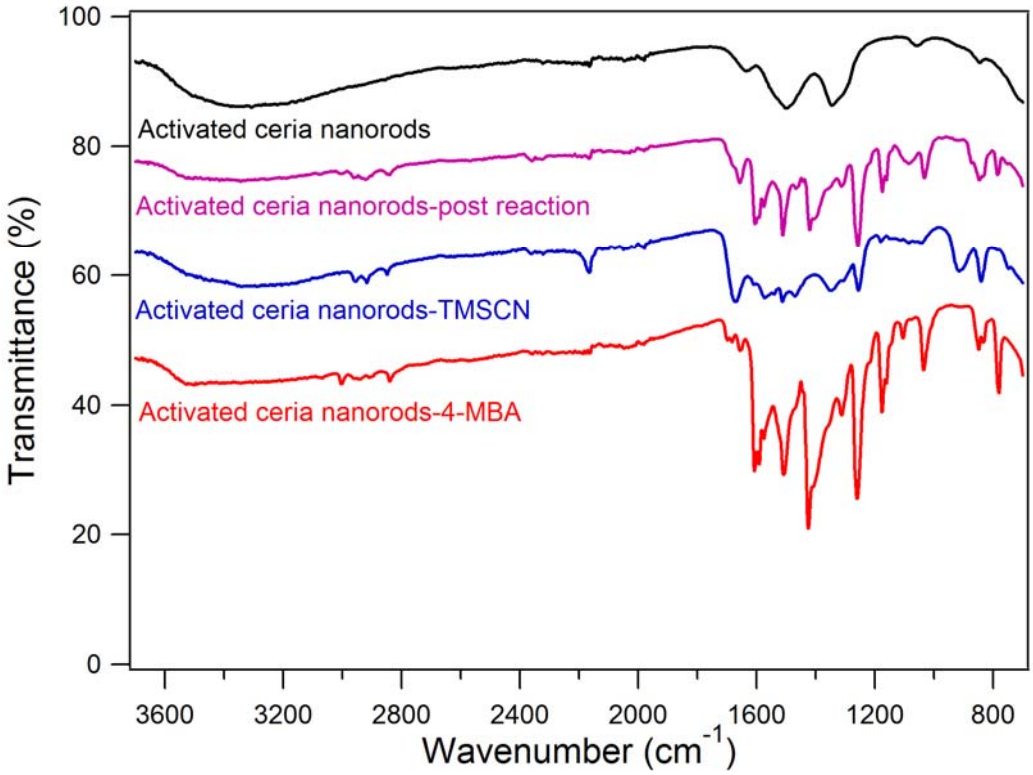

Fig. S14 FTIR spectra of activated ceria nanorods catalyst, the post-reaction catalyst, and the catalysts after impregnation in 4-MBA and TMSCN. The spectra are shifted downward for presentation clarity.

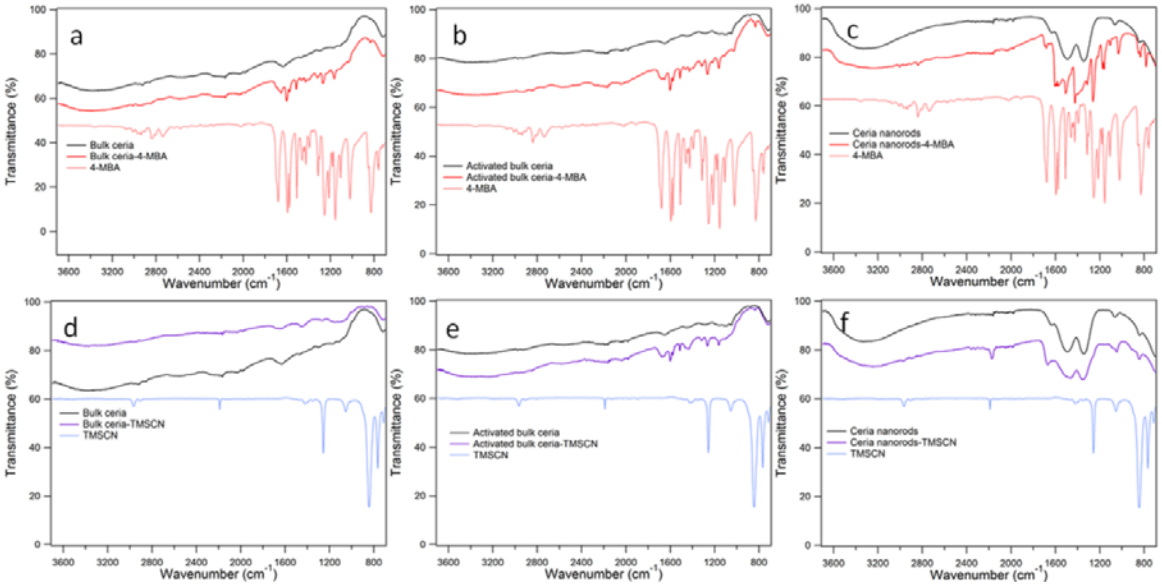

Fig. S15 FTIR spectra of bulk ceria, activated bulk ceria, unactivated ceria nanorods before and after impregnation in (a-c) 4-MBA or (d-f) TMSCN. The spectra of 4-MBA and TMSCN are displayed for comparisons. The spectra are shifted downward for presentation clarity.

Table S2 The infrared absorption frequency correlation table for the infrared spectra in Fig. 3, S14 and S15.

Wavenumber (cm^{-1})	**Vibration[1,2]**
3000-2800	CH_3 C–H stretch
2740	C-H stretch in aldehyde
2190, 2166	C≡N stretch
1680	C=O stretch in aldehyde
1606, 1591, 1508	C-C stretches in the benzene ring
1419	CH_3 twist
1356	CH_3 wag
1257	Si–CH_3 umbrella
1055	Si–O–Si asymmetric stretch
912	Silanol Si–O stretch
841	Si–CH_3 rock

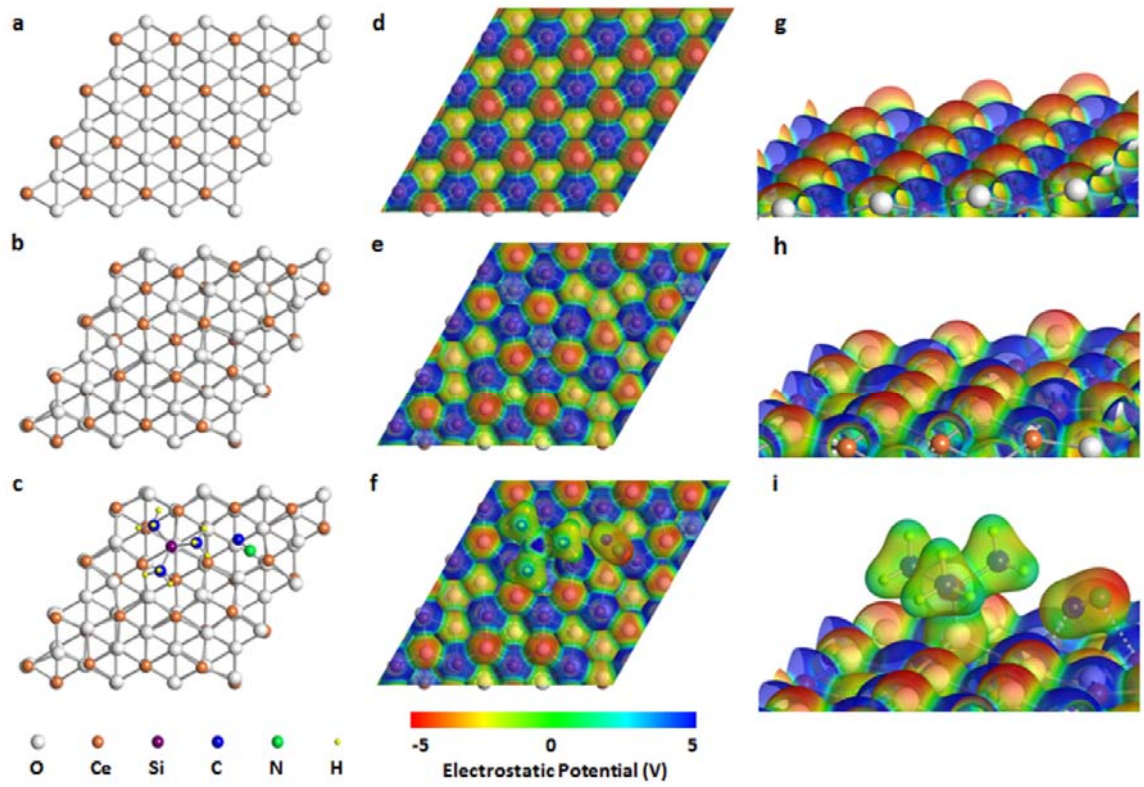

Fig. S16 Structures of (a) CeO_2 slab, (b) CeO_{2-x} slab and (c) TMSCN adsorbed on the CeO_{2-x} slab. Isosurfaces of electron density (isovalue = 0.2 electron/Å^3) of the three models color-coded with the electrostatic potential are illustrated from (d, e, f) top view and (g, h, i) zoomed-in angled view, respectively. The negative electrostatic potential around O-sites illustrates that O atoms are negatively charged, particularly that the surface O atoms are even more negatively charged than the subsurface ones. The positive electrostatic potential around Ce-sites suggests that the Ce atoms are positively charged.

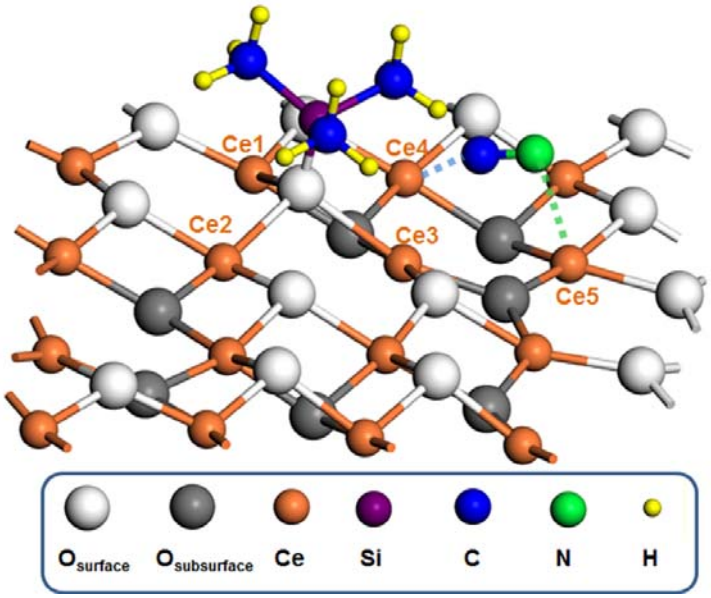

Fig. S17 Side view of the optimized structure of a TMSCN molecule chemisorbed on the CeO_{2-x} slab in the ball-and-stick representation.

Table S3 Interatomic bond lengths (Å) in CeO_{2-x} slab, TMSCN and TMSCN adsorbed on the CeO_{2-x} slab model.

Interatomic bond lengths (Å)	Ce(1)-O	Ce(2)-O	Ce(3)-O	O-Si	Si-C (N)	C-N	Ce(4)-C	Ce(5)-N
CeO_{2-x}	2.48	2.37	2.49	–	–	–	–	–
TMSCN	–	–	–	–	1.86	1.17	–	–
TMSCN adsorbed on CeO_{2-x}	2.61	2.62	2.74	1.68	4.57	1.19	2.82	2.66

Table S4 Binding energies and atomic charges of individual atoms in the adsorption models.

Models	Binding Energy (eV)	Charge (|e|)								
		Ce(1)	Ce(2)	Ce(3)	O	Si	C(N)	N	Ce(4)	Ce(5)
CeO_{2-x}		2.69	2.68	2.74	–1.65	-	-	-	2.86	2.76
TMSCN	–6.28	-	-	-	-	1.51	–0.28	–0.27	-	-
TMSCN adsorbed on CeO_{2-x}	–1.08	2.62	2.66	2.70	–1.42	1.54	–0.36	–0.51	2.85	2.78
CN detached from TMSCN- CeO_{2-x}	4.15	-	-	-	-	-	–0.44	–0.23	-	-
CN adsorbed on CeO_{2-x}	–5.25	2.69	2.71	2.80	–1.64	-	–0.36	–0.54	2.86	2.78
TMS adsorbed on CeO_{2-x}	–2.11	2.61	2.64	2.72	–1.42	1.53	-	-	2.83	2.69

References

(1) Smith, B. C. *Infrared spectral interpretation: a systematic approach*; 1st ed.; CRC Press LLC: Boca Raton, Florida, 1998.
(2) Thirupathi, B.; Patil, M. K.; Reddy, B. M. *Appl. Catal. A* 2010, **384**, 147-153.